Materials Science and Engineering B 176 (2011) 217–226

Contents lists available at ScienceDirect

Materials Science and Engineering B

journal homepage: www.elsevier.com/locate/mseb

Refining of metallurgical silicon by directional solidification

M.A. Martorano[a,*], J.B. Ferreira Neto[b], T.S. Oliveira[a], T.O. Tsubaki[b]

[a] Department of Metallurgical and Materials Engineering, University of São Paulo, Av. Prof. Mello Moraes, 2463 São Paulo-SP, 05508-900, Brazil
[b] Laboratory of Metallurgy and Ceramics Materials, Institute for Technological Research, Av. Prof. Almeida Prado, 532, São Paulo-SP, 05508-901, Brazil

ARTICLE INFO

Article history:
Received 11 June 2010
Received in revised form
29 September 2010
Accepted 21 November 2010

Keywords:
Silicon
Metallurgical silicon
Solar silicon
Refining
Directional solidification
Solar cells

ABSTRACT

The directional solidification of a typical and a previously refined metallurgical silicon was carried out in a vertical Bridgman furnace. The mold velocity out of the hot zone of the furnace changed from one experiment to another in the range between 5 and 110 $\mu m\,s^{-1}$. Samples were extracted from the cylindrical ingots obtained in the experiments to investigate the effects of the mold velocity on the micro and macrostructures and on the concentration profiles of impurities along the ingots. At the lowest mold velocity, the macrostructures consist of columnar grains oriented approximately parallel to the ingot axis. As velocity increases, grains become thinner and more inclined in the radial direction. Precipitated particles containing Si, Fe, Al, and Ti are observed at the top of all ingots and, as the mold velocity increases, they are also seen at the ingot bottom and middle. The concentration profiles of several impurities have been measured along the ingots by inductively coupled plasma atomic emission spectrometry (ICP), indicating an accumulation of impurities at the ingot top. Consequently, the bottom and middle of the ingots are purer than the corresponding metallurgical silicon from which they solidified. Slices from the ingot bottom have also been analyzed by the glow discharge mass spectrometry technique (GDMS), allowing measurement of impurity concentrations that were below the quantification limit of the ICP. The purification effect and the accumulation of impurities at the ingot top are more pronounced as the mold velocity decreases. In the ingots obtained from the typical metallurgical silicon at the lowest mold velocities (5 and 10 $\mu m\,s^{-1}$), except for Al, all impurities are in concentrations below an important maximum limit for the feedstock of solar grade silicon. At the same mold velocities, the concentrations of Fe, Ti, Cu, Mn, and Ni measured at the bottom of the ingots obtained from both types of metallurgical silicon (typical and previously refined) are even below some limits suggested directly for solar grade silicon.

1. Introduction

In the past decades, the increasing demand for solar grade silicon (SoG-Si) has triggered intensive research to develop alternative less expensive routes for its feedstock production [1–6]. The successful development of these alternative routes hinges upon the knowledge of the impurity content that can be tolerated, because lower Si purity and lower cell conversion efficiencies generally require less expensive processes [7,8]. Details about the effects of impurity elements on the SoG-Si properties can be found in recent reviews [9,10]. There is still no general agreement about the maximum impurity content in SoG-Si and its feedstock [11,12], but several authors have suggested maximum concentration limits [11–17], some of which are given in Table 1. Hopkins et al. [18] determined the impurity content limits (C_S in Table 1) in Si cells to attain efficiencies at least 90% of those in cells traditionally produced by the Czochralski method, which were about 10.3%. This efficiency (≈9.3%) can be obtained using feedstock with an impurity concentration higher than C_S, as calculated by Bathey and Cretella [16] considering the segregation that occurs during solidification in the Czochralski furnace (C_f in Table 1).

An important alternative route for SoG-Si production is the so-called "metallurgical route", whereby the metallurgical grade silicon (MG-Si), with typical purity of 98.5% Si [19] (Table 1), is refined by a combination of steps including directional solidification [3,6,20–22]. During solidification, many impurities are segregated to the melt, resulting in a purer solid. The difference between impurity concentrations in solid and melt is quantified by the solute partition coefficient, also known as the equilibrium segregation coefficient, which is defined as $k = C_s/C_l$, where C_s and C_l are the equilibrium impurity concentrations in the solid and liquid, respectively, at a given temperature. Values of k for several types of important impurities in Si are given in Table 1 [18,23–26]. As a result of segregation to the melt, all impurities other than B, P, O, and C, experience severe macrosegregation in the solid during solidification, because $k \ll 1$. Nevertheless, segregation of B and P has also been reported after directional solidification of Si [27,28].

* Corresponding author. Tel.: +55 11 3091 6032; fax: +55 11 3091 5243.
E-mail addresses: martoran@usp.br (M.A. Martorano), jbfn@ipt.br (J.B.F. Neto), theo.usp@bol.com.br (T.S. Oliveira), tomoe@ipt.br (T.O. Tsubaki).

0921-5107/$ – see front matter © 2010 Elsevier B.V. All rights reserved.
doi:10.1016/j.mseb.2010.11.010

Table 1
Maximum impurity concentration in final solid Si (C_s) and in its feedstock (C_f), assuming growth by a single pull in a Czochralski furnace and an efficiency of 90% relative to that of conventional solar cells. Suggestions for impurity contents in SoG-Si (C_{SoG}), the typical composition of MG-Si (C_{MG}), and the solute partition coefficient (equilibrium segregation coefficient) k are also shown.

Element	C_s (atoms/cm^{-3})	C_s (ppmw)	C_f[c] (ppmw)	C_{SoG} (ppmw)	C_{MG}[f] (ppmw)	k
Fe	6.5×10^{14}[a]	0.026[a]	370	<1[d]	300–25,000	8×10^{-6}[g]
Al	2.0×10^{16}[a]	0.38[a]	0.64	0.005–0.05[d]	300–5000	2×10^{-3}[g]
Cu	1.5×10^{16}[a]	0.68[a]	4500	–	5–100	4×10^{-4}[g]
Ti	2.0×10^{12}[a]	2.9×10^{-4}[a]	19	<1[e]	100–1000	3.6×10^{-6}[a]
V	9×10^{11}[a]	1.8×10^{-5}[a]	4.0	–	1–300	4×10^{-6}[a]
Mn	4.5×10^{14}[a]	0.018[a]	149	–	10–300	10^{-5}[g]
Cr	2.5×10^{14}[a]	9.3×10^{-3}[a]	133	<1[e]	5–150	1.1×10^{-5}[a]
Ni	2.5×10^{15}[a]	0.10[a]	1970[b]	–	10–100	8×10^{-6}[h]
B	10^{17}[b]	0.77[b]	–	0.1–10[d]	5–70	0.72[i]–0.8[g]
O	–	–	–	10–20[d]	100–5000	0.2–1.25[j]
C	2.5×10^{16}[b]	0.21[b]	–	0.5–1[d]	50–1500	0.034–0.3[j]
Ca	–	–	–	<2[e]	20–2000	–
Mg	–	–	–	–	5–200	–
Zr	10^{12}[b]	6.5×10^{-5}[b]	325	–	5–300	–
Mo	10^{12}[b]	6.8×10^{-5}[b]	66	–	1–10	–
W	–	–	1153	–	–	–
Co	–	–	193	–	–	8×10^{-6}[g]
Ta	3×10^{12}[b]	3.9×10^{-4}[b]	142	–	–	10^{-7}[g]
P	10^{17}[b]	0.77[b]	12	0.02–2[d]	5–100	0.35[g]
Nb	–	–	9.3	–	–	–

[a] Ref. [18]: the solute partition coefficients presented by these authors were referred to as effective coefficients, which might be equal to or larger than the actual equilibrium coefficients.
[b] Ref. [15]: C_s was obtained from Fig. 12 in [15].
[c] Ref. [16].
[d] Ref. [17].
[e] Ref. [11].
[f] Ref. [19].
[g] Ref. [23].
[h] Ref. [24].
[i] Ref. [25].
[j] Ref. [26]: a range of solute partition coefficients, reported by different authors, was presented for O and C.

Therefore, the first part of the ingot to solidify is much purer than the parts that solidified later.

The purification of MG-Si has been examined in several directional solidification processes. The minimum content of most impurities in the resulting ingot was significantly lower than that in the MG-Si feedstock, as given in Table 2 for different processes: Czochralski [29,30], the heat exchanger method (HEM) [31,32], simple crucible extraction from the furnace [20], and an unspecified directional solidification method [7,33]. In the Czochralski furnace, Kuroda and Saitoh [30] reported growth rates from 3 to 33 $\mu m\,s^{-1}$ at a temperature gradient of about 20 K cm^{-1}. For the HEM, Khattak et al. [31] reported a growth velocity of $\approx$14 $\mu m\,s^{-1}$. The remaining authors did not give the solidification conditions and none of these authors showed detailed profiles of impurity concentrations along the ingots.

The objective of the present work is to study the effect of different growth velocities on the concentration profile of impurities and on the micro-macrostructures of Si ingots grown in a vertical Bridgman furnace from metallurgical grade silicon (MG-Si). Detailed solidification conditions, such as the growth velocity and temperature gradient, and the concentration profiles of several impurities along the ingots are given and analyzed. To the authors' knowledge, this type of data is not available in the literature. The vertical Bridgman furnace was chosen, because it has been exhaustively used in fundamental studies of solidification and the mold velocity and temperature gradient can be accurately controlled.

2. Directional solidification experiments

Cylindrical ingots were obtained in a vertical Bridgman furnace by melting and solidifying metallurgical grade Si feedstock either as-received from the manufacturer (MG-Si) or previously refined (RMG-Si) with synthetic slags, oxygen injection, and acid leaching (Table 3). The feedstock was inductively melted under high purity argon (99.999% Ar) in a crucible of either high purity graphite or solar grade fused quartz located within the melting chamber of the Bridgman furnace (Fig. 1(a)). After melting, the liquid was poured into a cylindrical mold made of solar grade fused quartz tubes located within the solidification chamber of the furnace. The inner surface of the tubes (length 0.25 m, outer diameter 0.04 m, inner diameter 0.034 m) was coated with Si_3N_4 to facilitate the ingot removal after solidification. The quartz tubes were closed at its bottom end and supported by a set of 11 alumina discs (thickness 6 mm) resting on a metal rod that moved down at a carefully controlled withdrawal velocity (Fig. 1(b)). The quartz tube and discs were laterally supported by an outer zircon (zirconium silicate) shell with quartz powder in between. This whole system was placed within an annular cylindrical graphite susceptor heated by an induction field and used to transfer heat to the mold.

After pouring the liquid Si into the mold, followed by thermal stabilization for 45 min at 1500 °C, the base and metal rod supporting the system began to move down at a controlled velocity, withdrawing the mold out of the susceptor. When moving down, the system crossed a graphite baffle, designed to separate the hot and cold zones of the furnace, entering the cold zone formed by a water cooled serpentine. A type-B thermocouple (Pt–6%Rh/Pt–30%Rh) was fixed relative to the susceptor to control the system temperature. In one of the experiments, two thermocouples were located parallel to the quartz mold tube, with the measuring junction adjacent to the mold outer surface to estimate the temperature gradient within the metal. This gradient varied between 10 and 20 K cm^{-1} in the temperature range of 1300–1414 °C, at the withdrawal velocity of 10 $\mu m\,s^{-1}$. The experimental conditions were designed to show the effect of the withdrawal velocity of the mold ($5 \le V \le 110\ \mu m\,s^{-1}$) on the impurity concentration profiles along the ingots grown from either the MG-Si or the RMG-Si.

Table 2
Impurity contents (ppmw) in Si ingots solidified at a given growth velocity (V) from MG-Si feedstock by different directional solidification processes: Czochralski (CZ); heat exchanger method (HEM); uncontrolled directional solidification (DS); and unspecified directional solidification (UDS).

Process	V(μm s^{-1})	Fe	Al	Cu	Ti	V	Mn	Cr	Ni	Ref.
CZ	–	<10	<10	<1	<0.1	<1	<0.1	<2	<1	[29]
CZ	8.3	2	60	0.2	0.04	–	–	0.1	–	[30]
CZ	18.3	60	200	2	10	–	4	1	–	[30]
HEM	14	15	12	5	1	3	10	1	1	[31]
HEM	14	7	4	1	1	3	10	1	1	[31]
HEM[a]	–	24	26	0.11	1.2	0.074	0.7	0.27	0.65	[32]
DS[b]	–	<10	<10	<10	–	–	–	–	–	[20]
UDS[c]	–	<10	<10	–	–	–	–	–	–	[33]
UDS[c]	–	<2	2.5	–	<7.3	–	–	–	–	[7]
UDS[c]	–	18	4.9	–	<7.3	–	–	–	–	[7]
UDS[c]	–	3.4	2.0	–	<1	–	–	–	–	[7]

[a] Prior to directional solidification, the MG-Si feedstock was chemically refined to eliminate B and P, but others impurities were also eliminated; the authors claimed, however, that the major impurity content decrease was owing to the directional solidification in the HEM process.
[b] Directional solidification was carried out after chlorine chemical treatment of the MG-Si.
[c] The MG-Si feedstock was reported as high purity, because the impurity content was lower than the typical MG-Si.

Table 3
Chemical composition (ppmw) of feedstock: metallurgical grade Si as-received from the manufacturer (MG-Si) and previously refined (RMG-Si). The average of all chemical analyses (C_0 MG-Si) of slices of the ingots obtained from MG-Si and the quantification limit (QL) of elements for ICP are also given.

Feedstock	Fe	Al	Cu	Ti	V	Mn	Cr	Ni	Ca	Mg	Na	Zr	Zn	Total
MG-Si	2800	690	240	140	5.7	69	100	60	680	11	10	17	2.4	4825
C_0 MG-Si	2916	320	255	146	14.7	67	111	183	–	–	–	30	–	–
RMG-Si	18	8	<17	<7	<3.3	<8.3	<7	<7	2.2	1.1	<1.5	<7	<1	<57.8
QL	7	7	17	7	3.3	8.3	7	7	–	–	–	7	–	–

3. Characterization of samples

At the end of an experiment, each cylindrical ingot (length ≈0.25 m, diameter ≈0.034 m) was stripped out of the quartz mold and sectioned transversally in about 10 slices of approximately equal thickness. These slices were then sectioned longitudinally, giving rise to two samples: one for chemical analysis and the other for micro and macrostructural examination.

To reveal the microstructure, samples were ground, polished (using colloidal silica), and finally examined in an optical and a scanning electron microscope (SEM) equipped with a microprobe with energy dispersive spectroscopy (EDS). The grain macrostructure was revealed by etching samples with an aqueous solution of 50 wt.% NaOH for 10 s at the temperature of 90 °C.

The chemical analyses of all slices cut off from each ingot were used to construct concentration profiles of all elements as a function of the distance along the ingot length. For the chemical analysis of each slice, 3 g were first dissolved in a solution consisting of 5 ml HNO_3 (65% P.A.) and 15 ml HF (48% P.A.) and then analyzed by inductively coupled plasma atomic emission spectrometry (ICP) in a Shimadzu ICPS-7500 system, giving the average concentration of elements in the slice. A quantification limit (QL) was estimated

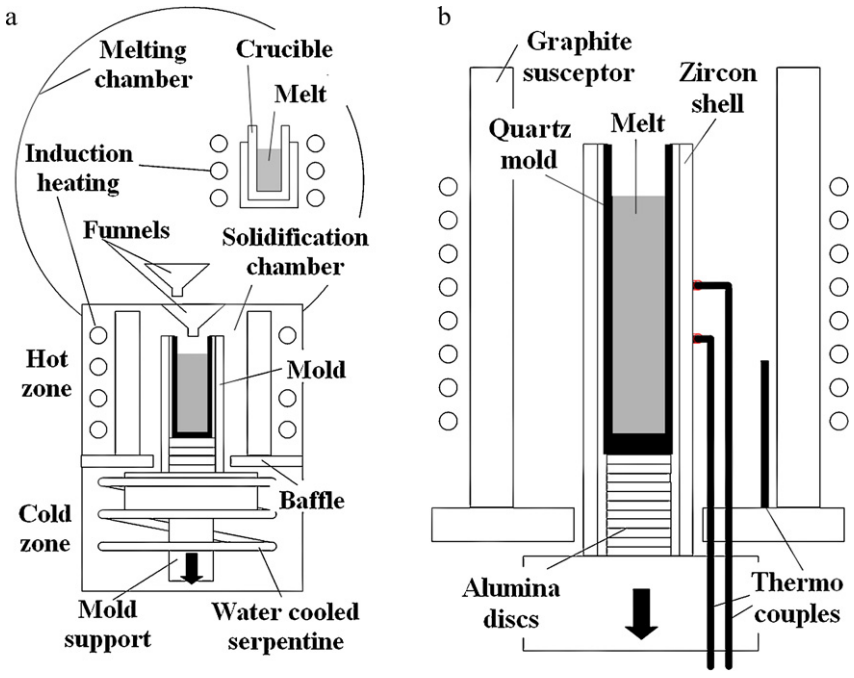

Fig. 1. Schematic view of the Bridgman furnace for directional solidification: (a) melting and solidification chambers; (b) detail of the directional solidification mold, showing two lateral thermocouples used in one of the experiments to measure the temperature gradient.

for each element by analyzing a series of standard solutions with decreasing concentrations of elements. In the series, the measured concentration of each element decreased to an approximately constant value, no longer changing significantly for solutions of lower concentrations. This constant value was actually the blank concentration with a superimposed background noise. The QL given in Table 3 was defined as three times this constant concentration value. Moreover, the standard deviation of the blank concentration was used to calculate the quantification limit recommended by the IUPAC [34]. The IUPAC limit, however, was always lower than the QL presented in Table 3, which was finally adopted in an attempt to improve the quantification methodology carried out in the present work.

The average concentration (C_0 MG-Si in Table 3) of each element in all slices obtained from all ingots grown from MG-Si is compared with the concentration of the MG-Si as received from the manufacturer. The agreement between the two types of analysis was good for five elements (Fe, Cu, Ti, Mn, Cr), but poor for the remaining four elements (Al, V, Ni, Zr). Increasing the number of analyzed slices would probably improve this agreement. Chemical analyses by the glow discharge mass spectrometry technique (GDMS) were also carried out on a region of approximately 18 mm^2 of the surface of slices cut from the bottom of the ingots, near the center of their transversal section.

4. Macro and microstructures of silicon ingots

The macrostructures of the longitudinal section (parallel to the mold movement direction) of some of the ingots are shown in Fig. 2. Actually these are formed from the macrographs of individual slices, because a longitudinal section of the whole ingot could not be obtained without fragmentation. In some of the ingots, grains in one slice do not seem to match those of the adjacent slice, because some small part of the ingot in between the two slices might have fragmented during sawing. Two slices in Fig. 2(d) were completely fragmented and, therefore, were not included in the image, but an empty space was left to indicate it.

The macrostructures of ingots obtained from both MG-Si and RMG-Si at the slowest velocity ($V = 5\,\mu m\,s^{-1}$) consist of columnar grains oriented approximately parallel to the direction along which the mold was withdrawn from the furnace (Fig. 2(a) and (b)). Since columnar grains grow approximately parallel to the heat flux direction, it is possible to conclude that solidification occurred directionally. Close to the mold wall, grains are slightly inclined in the radial direction, indicating that radial heat extraction was also important during solidification at this position. Actually, the axial temperature gradient that gives rise to the axial heat flux originates mainly from the radial heat conduction, since the base of the quartz mold was isolated by the alumina discs (Fig. 1(b)).

When V increased from 5 to 20 $\mu m\,s^{-1}$ for RMG-Si (Fig. 2(b) and (c)), columnar grains became thinner as a result of the larger cooling rate. The cooling rate in the system, R, might be estimated by $R = VG$, where V is the growth velocity and G is the temperature gradient [35]. Considering that G was kept approximately constant, the cooling rate increased fourfold ($\approx$0.01–0.04 $K\,s^{-1}$), increasing the nucleation rate of columnar grains and eventually making them thinner. For a further increase in V from 20 to 110 $\mu m\,s^{-1}$ (Fig. 2(c) and (d)), grains became more inclined and perpendicular to the mold wall, indicating that the importance of radial heat conduction increased.

Micrographs of ingots obtained in the scanning electron and optical microscopes are given in Figs. 3 and 4, respectively. Neither a dendritic nor a cellular structure was clearly observed in any ingot. However, owing to the relatively low concentration of elements, even if a dendritic or a cellular structure existed during solidification, they would not have been revealed by the chemical etching or by the backscattered electron contrast of SEM.

Precipitates were observed in different parts of the ingots depending on the mold velocity and feedstock material. The larger amount of precipitates in a certain region is a result of the larger impurity content at that region, because these precipitates are rich in impurity elements. Table 4 shows the distribution of ingot precipitates for all mold velocities and feedstock materials, generally indicating an accumulation of impurities at the top, which was the last part to solidify. In all ingots, precipitates were observed at the top, whereas further precipitates at the bottom and middle (i.e., throughout the ingot) were seen only in the following mold velocities and feedstock materials: (a) 20 $\mu m\,s^{-1}$, for MG-Si; and (b) 110 $\mu m\,s^{-1}$, for both MG-Si and RMG-Si.

The top of the ingot solidified from MG-Si at the slowest mold velocity (5 $\mu m\,s^{-1}$) shows a layer of precipitates of about 2 mm thickness (Fig. 3(a)). The precipitates within and below the layer are presented in detail in Fig. 3(b) and (c), respectively. The SEM images suggest the existence of more than one type of intermetallic, shown by different tones of grey. The electron microprobe analyses (EDS) of the precipitates revealed different contents of the following elements: Si, Fe, Al, Ti, Cr, Ni, Cu, Zr, and P. Except for P, all other elements were also found by Vogelaar [36] in several precipitates present in commercially cast ingots of MG-Si. At the same mold velocity (5 $\mu m\,s^{-1}$), the top of the ingot obtained from RMG-Si showed only small precipitates, rather than a continuous layer, which is a result of the higher purity of RMG-Si compared with MG-Si.

When mold velocity increased, precipitates tended to be more uniformly distributed along the whole ingot and less concentrated at the top. The ingots solidified from MG-Si at the fastest mold velocities (20 and 110 $\mu m\,s^{-1}$) showed precipitates at the bottom, middle, and top of the ingots (Table 4); in the middle, for example, isolated strings of precipitates were observed for 110 $\mu m\,s^{-1}$ (Fig. 4(a)). At the same mold velocity, however, the middle part of the ingot grown from RMG-Si showed only isolated precipitates (Fig. 4(c)) owing to its higher purity.

5. Effect of mold velocity on profiles of impurity concentration

During directional solidification of liquid Si in which a planar solid–liquid interface moves towards the liquid, solid layers form continuously. This solidified layer is purer (for most impurities) than the liquid from which it forms and, therefore, it rejects impurities to the adjacent liquid, creating a liquid layer enriched with impurity elements. The impurities in this layer diffuse towards the bulk liquid with or without the help of liquid convective movement, eventually accumulating at the ingot end. The severity of this accumulation depends on different parameters, namely, the solute partition coefficient, the impurity diffusivity in the melt, the convection pattern in the liquid, and the solidification velocity, which is one of the most important parameters [35]. An increasing velocity might decrease the accumulation of impurities at the last portion of the ingot to solidify as a result of two major effects: (a) a compression of the enriched solute layer adjacent to the solid–liquid interface, decreasing its interaction with the convective bulk liquid movement and eventually decreasing the solute transport and its accumulation at the ingot end [37]; (b) the possible growth of instabilities at the planar solid–liquid interface, which might evolve into a cell or dendritic pattern that hinders the solute transport into the bulk liquid, decreasing its accumulation at the ingot end [38].

To examine the result of this redistribution process for several important impurities in Si, concentration profiles of Fe, Al, Cu, Ti, V, Mn, Cr, Ni, and Zr along the length of the cylindrical ingots were con-

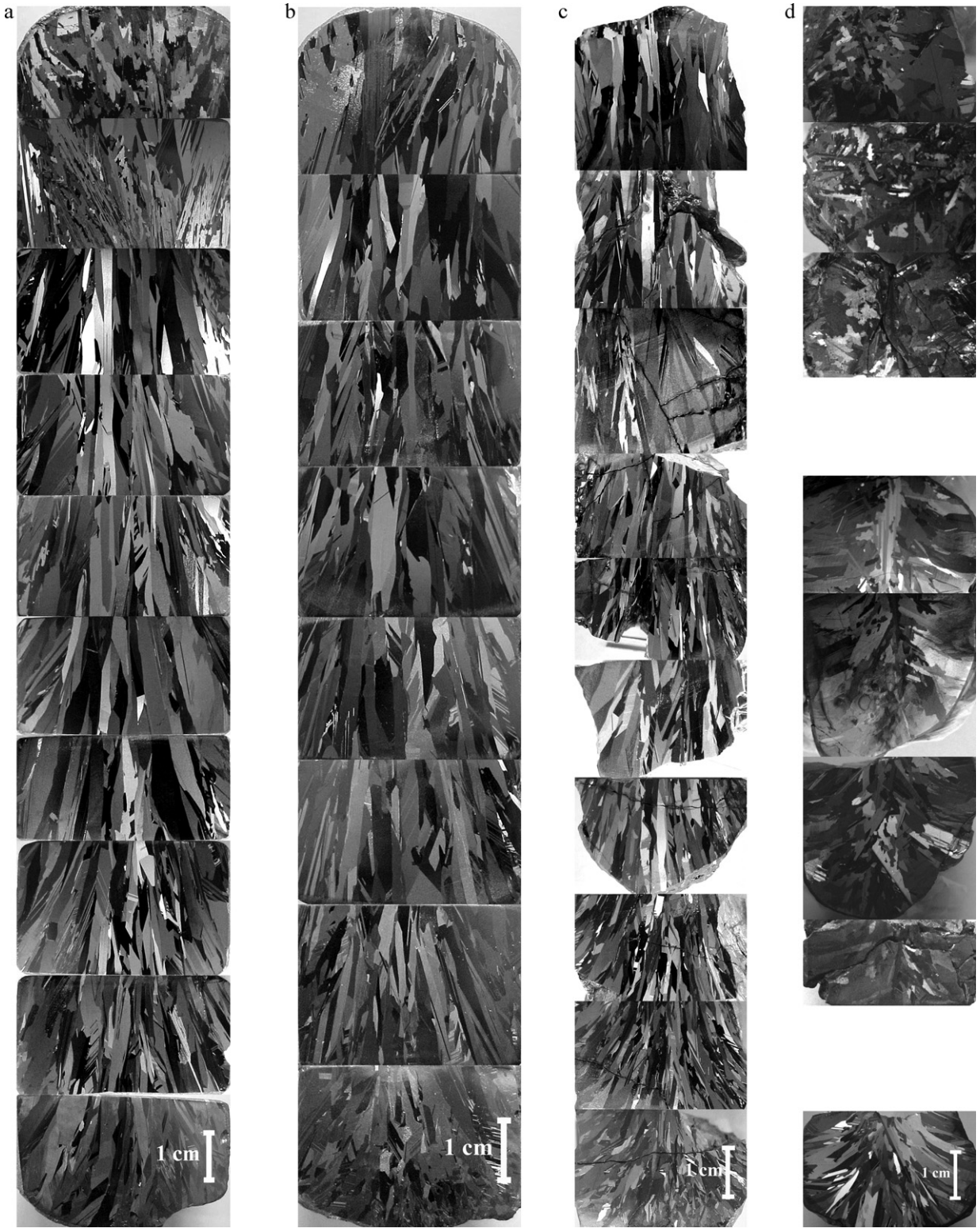

Fig. 2. Macrostructures of Si ingots: (a) MG-Si, $V = 5\ \mu m\ s^{-1}$; (b) RMG-Si, $V = 5\ \mu m\ s^{-1}$; (c) RMG-Si, $V = 20\ \mu m\ s^{-1}$; (d) RMG-Si, $V = 110\ \mu m\ s^{-1}$.

structed for different mold velocities using the ICP analyses of the ingot slices (Fig. 5). Each profile is given as a function of the dimensionless distance from the ingot bottom, using the ingot length as the reference scale. One Fe profile shown in Fig. 5(a) and the Al profiles given in Fig. 5(c) are for the experiments with RMG-Si, whereas all other profiles are for ingots grown from MG-Si. An attempt was also made to construct profiles for all the other ingots grown from RMG-Si, but the concentrations measured with ICP were all below the QL (except for those in the slice at the top of the ingot) and, consequently, these profiles are not presented.

The GDMS technique enabled the measurement of concentration values that were below the QL of the ICP. Only the bottom slices from the ingots grown at mold velocities 5 and 10 $\mu m\ s^{-1}$ were analyzed by GDMS (Table 5), because these were free from precipitates.

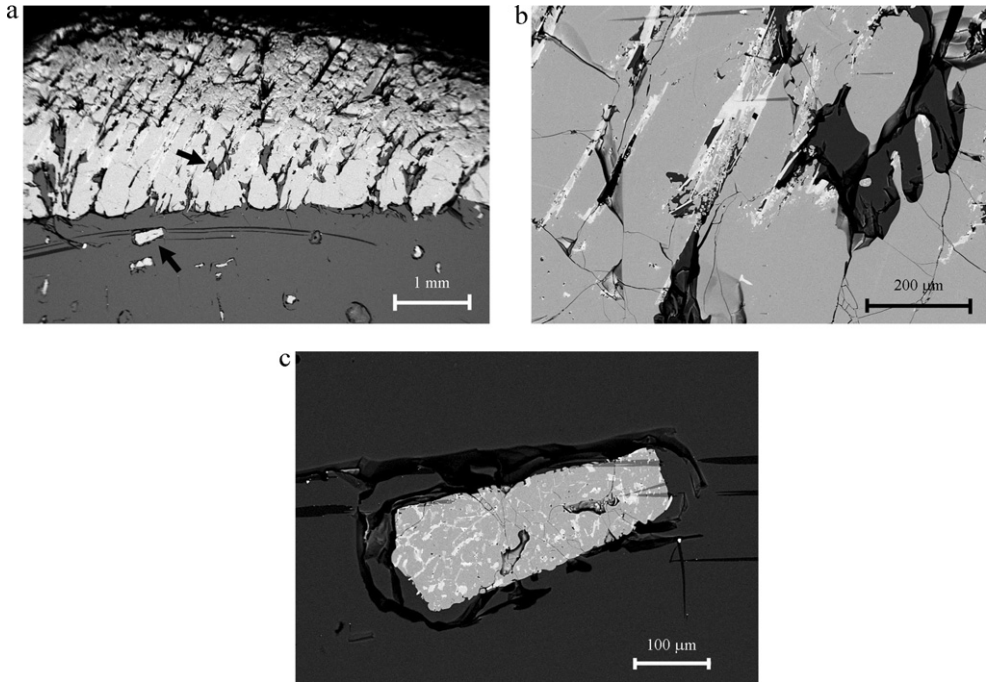

Fig. 3. Microstructures obtained in backscattered electron contrast (SEM) of a sample from the top of the Si ingot solidified from MG-Si at the mold velocity $V = 5\ \mu m\ s^{-1}$: (a) top layer of precipitates; (b) detail of precipitates indicated in (a) by arrow within the layer; (c) precipitate indicated in (a) by arrow below the top layer.

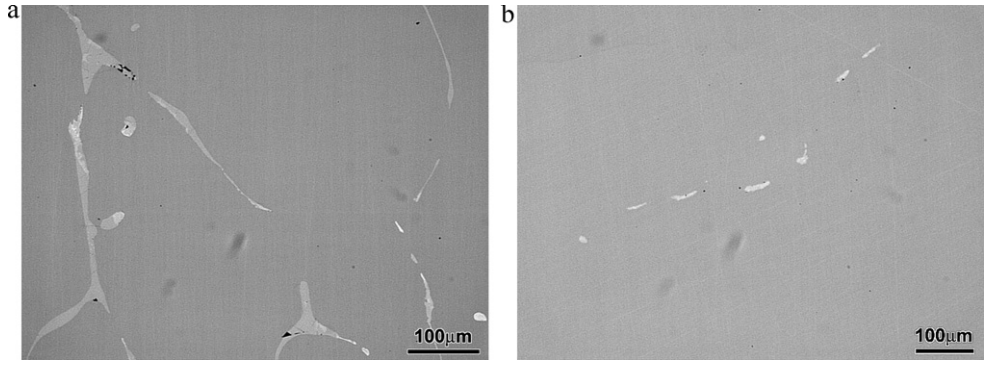

Fig. 4. Microstructures obtained in optical microscope of samples from the middle of ingots grown at $V = 110\ \mu m\ s^{-1}$ from (a) MG-Si and (b) RMG-Si.

Table 4
Indication of the presence (Y) or absence (N) of precipitates at the bottom, middle, or top of Si ingots directionally solidified at different mold velocities (V) from either metallurgical grade (MG-Si) or previously refined metallurgical grade silicon (RMG-Si).

	V ($\mu m\ s^{-1}$)							
	MG-Si				RMG-Si			
	5	10	20	110	5	10	20	110
Top	Y[a]	Y	Y	Y	Y	Y	Y	Y
Middle	N	N	Y	Y[a]	N	N	N	Y[a]
Bottom	N	N	Y	Y	N	N	N	Y

[a] Microstructures for these regions of the ingot are shown in Figs. 3 and 4.

Table 5
Chemical analysis (ppmw) by GDMS of slices at the bottom of ingots grown from either MG-Si or RMG-Si at $V = 5$ and $10\ \mu m\ s^{-1}$. The minimum theoretical concentrations (kC_0, in which k was obtained from Table 1) are also shown for each type of feedstock material.

Ingot-V ($\mu m\ s^{-1}$)	Fe	Al	Cu	Ti	V	Mn	Cr	Ni	Zr
MG-5	0.14	0.5	<0.05	0.002	<0.001	<0.005	0.026	0.026	<0.05
MG-10	0.29	0.56	<0.05	<0.001	0.003	0.009	0.021	0.058	<0.05
kC_0^{MG}	0.023	0.64	0.10	5.3×10^{-4}	5.9×10^{-5}	6.7×10^{-4}	0.0012	0.0015	–
RMG-5	0.17	0.98	<0.05	0.004	0.003	0.05	0.014	0.024	<0.05
RMG-10	0.47	0.036	0.061	<0.001	0.002	0.011	0.012	0.027	<0.05
kC_0^{RMG}	1.4×10^{-4}	0.016	$<3.2 \times 10^{-3}$	2.9×10^{-5}	$<6 \times 10^{-6}$	$<1.5 \times 10^{-5}$	2.8×10^{-5}	$<1.2 \times 10^{-5}$	–

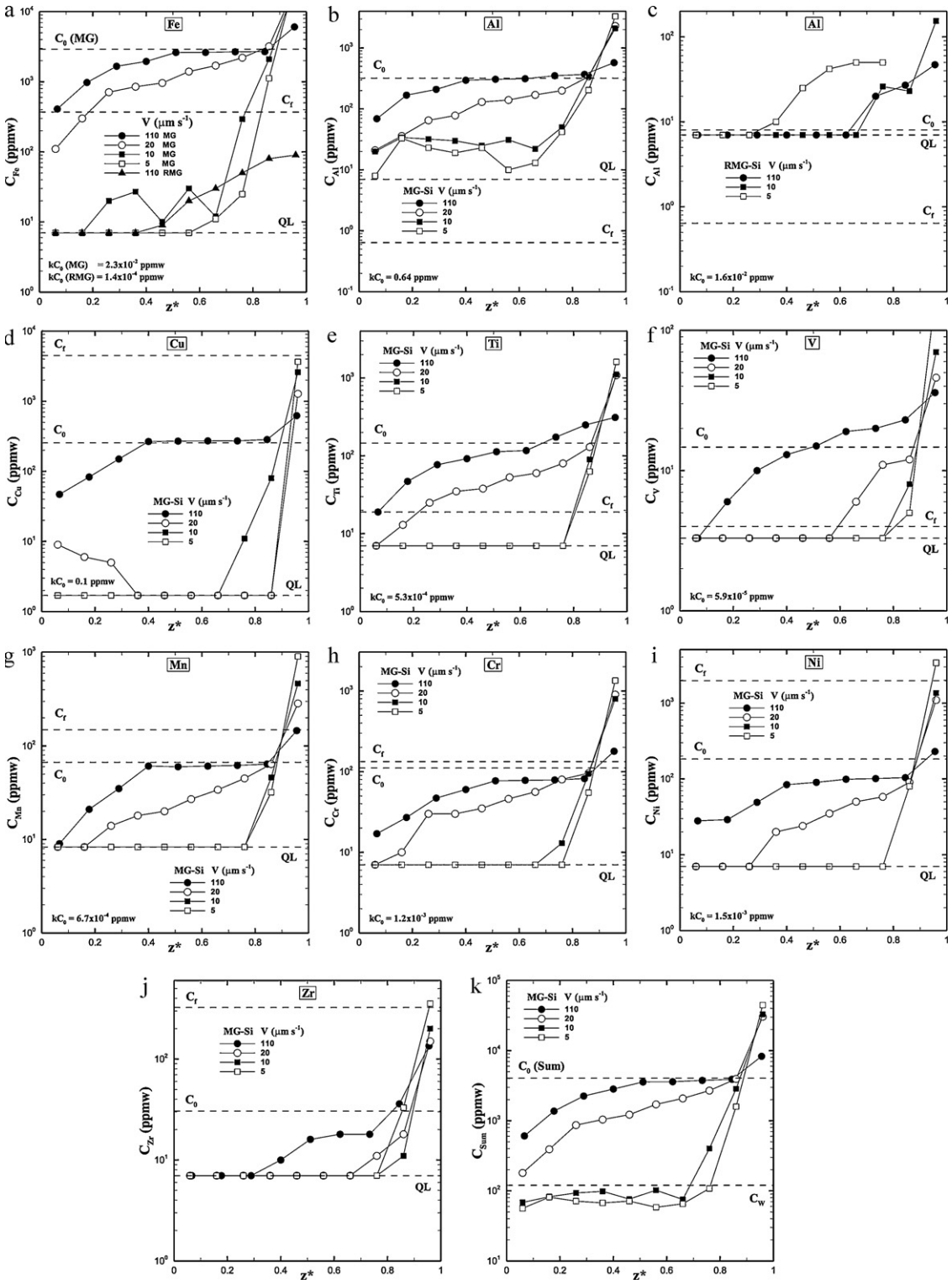

Fig. 5. Concentration of elements as a function of the distance z^* (normalized by the ingot length) from the bottom of ingots grown from either MG-Si or RMG-Si at $V = 5$, 10, 20, and 110 μm s^{-1}. Profiles for the following elements are shown: (a) Fe; (b) Al; (c) Al (RMG); (d) Cu; (e) Ti; (f) V; (g) Mn; (h) Cr; (i) Ni; (j) Zr; and (k) sum of concentrations of all elements (C_{Sum}). Also shown are: the average concentration of each element (C_0), the quantification limit (QL), and the maximum concentration recommended for SoG-Si feedstock (C_f) given in Table 3. The maximum total impurity content (C_W) suggested by Wakefield et al., cited by Bathey and Cretella [16], and the minimum theoretical concentration (kC_0 in Table 5) are also shown for comparison purposes.

Since the GDMS was used to measure the impurity concentration of a relatively small surface area of the slice, the presence of precipitated particles separated by distances longer than or of the same order of magnitude as that of the analyzed region could complicate the analyses interpretation.

Although most of the impurity concentrations at the bottom slices are above the minimum theoretical concentration (kC_0 in Table 5), some of them, such as those of Fe and Al in the ingot grown from MG-Si at $V = 5$ μm s^{-1}, are below it, probably as a result of experimental errors in k or in the GDMS analyses.

All concentration profiles in Fig. 5 show an accumulation of elements at the top of the ingots, which was the last part to solidify. Therefore, the bottom half of these ingots (first part to solidify) is purer than its feedstock, with composition indicated by C_0. The values of C_0 for the MG-Si are the average of concentrations measured by ICP in all slices from all available ingots (C_0 MG-Si in Table 3). An accumulation at the last part to solidify, which is a characteristic of the so-called normal segregation, was expected, since $k<1$ for these impurities [37].

The concentration profiles of Fig. 5 show that a decrease in mold velocity increases purification and segregation of elements to the ingot top. This effect has already been explained by the model presented by Burton et al. [39] for the solidification with a planar solid–liquid interface. According to this model, at lower solidification velocities the thickness of the enriched solute layer of liquid increases, being more affected by the convective liquid movement occurring far from the interface, within the bulk liquid. Therefore, transport of impurities to the top of the ingot become more efficient with convection and the impurity accumulation in this region is increased. Kuroda and Saitoh [30] confirmed this effect for Si ingots grown in a Czochralski furnace (Table 2).

Yue and Clark [40] and Dean et al. [38] showed a similar effect in the directional solidification of Mg and Pb alloys. Nevertheless, they attributed the less intense accumulation of solute elements at higher mold velocities to a change in the solid–liquid interface morphology from planar to dendritic/cellular, decreasing the solute transport to the bulk liquid. In the present work, however, the existence of cells or dendrites at the higher mold velocities (20 and 110 $\mu m\,s^{-1}$) could not be confirmed. Although more evidence is still needed, precipitated particles observed along the whole ingot for these velocities is an indication of the presence of cells/dendrites, since impurities would be trapped in the liquid between them and precipitation would eventually occur until the end of solidification.

A comparison between the profiles of Fig. 5(a)–(c) can indicate the effect of the feedstock purity on the final distribution of impurity elements along the ingot. Generally, the concentration profiles for the ingots grown from RMG-Si (Fe in Fig. 5(a) and Al in Fig. 5(c)) showed values lower than those in the profiles obtained from the MG-Si at corresponding mold velocities. This was expected owing to the higher purity of RMG-Si. In Fig. 5(a), the Fe profile for the RMG-Si at 110 $\mu m\,s^{-1}$ has concentration values comparable to those of ingots grown from MG-Si at much lower velocities (5 or 10 $\mu m\,s^{-1}$). Consequently, the same level of purity can be obtained in ingots solidified from RMG-Si at 110 $\mu m\,s^{-1}$, or from MG-Si, a less pure feedstock material, but at lower mold velocities, namely, 5 and 10 $\mu m\,s^{-1}$.

The processing conditions during solidification of Si in the HEM, the Czochralski furnace, or in the present vertical Bridgman furnace are different. Nevertheless, the minimum concentrations of impurity elements in the profiles of Fig. 5 (Bridgman furnace) are similar to those given in Table 2 for Czochralski and HEM. The differences are reasonably explained by the variation in solidification velocity from one process to another. For example, the ingot solidified from MG-Si at the mold velocity of 110 $\mu m\,s^{-1}$ showed minimum concentrations (Fig. 5) of all elements but Al above those reported in Table 2. This difference can be a result of the larger mold velocity used in the present work experiments. When the mold velocity decreased to 20 $\mu m\,s^{-1}$, the minimum concentrations of Al, Cu, Ti, V, and Mn are in between those values reported in Table 2 for HEM at 14 $\mu m\,s^{-1}$ and Czochralski at 8.3 and 18.3 $\mu m\,s^{-1}$. For a further decrease in mold velocity to 10 or 5 $\mu m\,s^{-1}$, the GDMS analyses of the bottom slices (Table 5), which give the minimum concentrations in the ingots, showed that the contents of all impurity elements are below those reported in Table 2. Again, this can be explained by the lower mold velocity in the present work experiments when compared with those in Table 2.

6. Fulfilling the composition requirements for solar grade silicon

In Table 1 and Fig. 5, the maximum tolerable concentration of impurities calculated by Bathey and Cretella [16] for a feedstock to produce SoG-Si single crystals by Czochralski is indicated as C_f. At mold velocities of 5 and 10 $\mu m\,s^{-1}$, the concentration profiles of all impurities except Al (in MG-Si, Fig. 5(b)) are below C_f along 70% or more of each ingot. The theoretical minimum concentration of Al (kC_0), calculated from the composition of the MG-Si feedstock (Table 3), is equal to C_f (0.64 ppmw in Table 5). Consequently, the concentration of this element would never be adequate for SoG-Si feedstock after directional solidification of MG-Si. On the other hand, in MG-Si the initial concentrations (C_0) of Cu, Mn, Cr, Ni, and Zr were already below C_f before directional solidification, while those of Fe, Ti, and V decreased below C_f only after directional solidification. Therefore, decreasing the concentrations of the latter elements would be an important target of the directional solidification step to purify MG-Si. In this case, the mold velocity should not be higher than 10 $\mu m\,s^{-1}$ for a temperature gradient of approximately 20 $K\,cm^{-1}$.

To confirm that this lower range of mold velocities (5 or 10 $\mu m\,s^{-1}$) is adequate for MG-Si purification, Fig. 5(k) shows that the sum of concentrations (C_{Sum}) of all elements along approximately 70% of the ingots is below 120 ppmw, an upper limit suggested by Wakefield et al. (C_W), cited by Bathey and Cretella [16], for the feedstock of SoG-Si. Note that, to calculate C_T, when an impurity concentration in Fig. 5 was below the QL, this limit was adopted in the summation.

In the experiments with RMG-Si, concentration of all impurities except Al was already below C_f before directional solidification (see Table 3). The Al concentration decreased below C_f at the bottom slice of the ingot (GDMS analysis in Table 5) only after directional solidification at the mold velocity of 10 $\mu m\,s^{-1}$. Although this analysis is only for the bottom slice, there is a possibility that a larger part of the ingot could also have Al concentration below C_f. Therefore, except for a possible beneficial effect in reducing the Al content, purification of RMG-Si by directional solidification in the mold velocity range studied in the present work is unnecessary if C_f is adopted as the limit for SoG-Si feedstock.

This previous discussion stems from the composition requirements for the SoG-Si feedstock, which is further purified during the final steps of the SoG-Si ingot production by a process such as Czochralski. The following authors, however, proposed concentration limits directly to SoG-Si, rather than to its feedstock: (a) Hopkins et al. [18] and Pizzini [15] (C_s Table 1) proposed limits considering that the SoG-Si should have a 90% relative efficiency (see Introduction section); (b) Øvrelid et al. [13] suggested limits apparently based on the effects of impurities on the photovoltaic properties of a solar cell; and Yuge et al. [14] did not mention the criterion adopted to define their limits.

Three types of compositions obtained from the present work ingots can be compared with the impurity concentration limits suggested by these authors: (a) the theoretical minimum concentrations (kC_0 in Table 5); (b) the concentrations in the profiles of Fig. 5, obtained from the ICP analyses; and (c) the concentrations from the GDMS analyses of the slices at the bottom of the ingots obtained at the mold velocities of 5 and 10 $\mu m\,s^{-1}$ (Table 5).

For the ingots grown from MG-Si, the theoretical minimum concentration (kC_0^{MG} in Table 5) of Al is above the maximum limits suggested for SoG-Si by all four authors [13–15,18] mentioned previously. The theoretical minimum concentrations of Ti and V are also above the limits suggested by Hopkins et al. [18] and Pizzini [15] (C_s Table 1). Therefore, even if the present directional solidification was carried out under ideal conditions, these impurities would still depend on the further purification that occurs during

solidification in Czochralski crystal growth. On the other hand, the theoretical minimum concentrations of all the remaining impurities (Fe, Cu, Mn, Cr, Ni, Zr) fulfill all the suggested limits.

The portions of the concentration profiles above the QL for MG-Si (Fig. 5) show that no impurity element is below the limits suggested by Hopkins et al. [18] and Pizzini [15]. Nevertheless, some portion of the Fe profile for mold velocities 5 and 10 $\mu m\,s^{-1}$ is below the limit suggested by Øvrelid et al. [13]. For these two mold velocities, the GDMS analyses of the slices at the ingot bottom (Table 5) show that: (a) concentrations of Cu, Mn, and Ni are below the limits proposed by Hopkins et al. [18] and Pizzini [15]; (b) concentrations of Fe and Ti are below the maximum values proposed by Øvrelid et al. [13]; and (c) Ti concentration is also below the limit suggested by Yuge et al. [14].

The measured impurity concentrations in the ingots obtained from RMG-Si were generally lower than or approximately equal to those measured in the ingots from MG-Si, which can be explained by the higher purity of the RMG-Si. Therefore, the composition of the ingots grown from RMG-Si usually fulfilled at least the same composition requirements also fulfilled by the ingots from MG-Si. Owing to its higher purity, RMG-Si ingots also satisfied further concentration limits. For example, the theoretical minimum concentration of all analyzed impurities (kC_0^{RMG} in Table 5) are below all the maximum concentrations limits discussed previously. Therefore, if the present directional solidification step could be carried out under ideal conditions, the contents of all analyzed impurities in the resulting ingot would already be suitable for SoG-Si. The actual concentration profiles for the RMG-Si ingots (Fig. 5) do not allow any further conclusion from that already presented for the MG-Si ingots, because most of the impurity concentrations are below the QL of the ICP. The impurity concentrations measured by GDMS in the bottom slices of the ingots obtained at mold velocities 5 and 10 $\mu m\,s^{-1}$ (Table 5) show that, besides satisfying the same limits as those for the MG-Si ingots, the RMG-Si ingots had an Al concentration (for $V = 10\ \mu m\,s^{-1}$) below all the maximum limits discussed previously. Note, however, that the GDMS analysis is only for the slice cut from the ingot bottom.

7. Summary and conclusions

Cylindrical ingots were obtained by upward directional solidification of two types of feedstock materials: a metallurgical grade Si (MG-Si) and a previously refined metallurgical grade Si (RMG-Si). The directional solidification experiments were carried out in a vertical Bridgman furnace at a temperature gradient of approximately 20 $K\,cm^{-1}$ and at a constant mold velocity, which changed from one experiment to another in the range of 5–110 $\mu m\,s^{-1}$. The effects of changing the mold velocity were examined on the micro and macrostructures and concentration profiles along the ingots.

The ingots obtained from both MG-Si and RMG-Si at the slowest mold velocity (5 $\mu m\,s^{-1}$) show a macrostructure typical of directional solidification, i.e., columnar grains oriented approximately parallel to the cylindrical ingot axis. As the mold velocity increases up to 110 $\mu m\,s^{-1}$, columnar grains become thinner and more inclined in the radial direction. Although, a few precipitated particles are observed along the ingots obtained from MG-Si at the largest mold velocities (20 and 110 $\mu m\,s^{-1}$), there is not strong evidence of a dendritic or cellular structure within the grains.

In all ingots obtained in the present work, the part that solidified first (bottom) is purer than its feedstock material (MG-Si or RMG-Si), revealing an accumulation of all elements (Fe, Al, Cu, Ti, V, Mn, Cr, Ni, Zr) at the ingot top. The impurity contents along a large part of the length of the ingots generally decrease with a decreasing mold velocity, indicating a larger refining effect for lower velocities. For the ingots obtained from RMG-Si, this effect is more difficult to observe, because most of the concentration profiles are below the QL of the analytical technique.

Generally, the concentrations of elements in the ingots obtained from RMG-Si are lower than those measured in ingots from MG-Si solidified at the same mold velocities. The Fe profiles indicate that the same level or purity observed in the ingots grown from RMG-Si at the mold velocity of 110 $\mu m\,s^{-1}$ can be obtained from MG-Si at lower velocities, namely 5 and 10 $\mu m\,s^{-1}$. The minimum concentration of elements (found at the ingot bottom) in the ingots obtained from MG-Si at the mold velocity of 20 $\mu m\,s^{-1}$ are similar to those reported in ingots from the HEM and Czochralski at solidification velocities in the range between 8 and 18 $\mu m\,s^{-1}$. For a lower mold velocity (5 $\mu m\,s^{-1}$), the present work ingots are purer, while for a larger velocity (110 $\mu m\,s^{-1}$), ingots are less pure.

The contents of some impurity elements (Cu, Mn, Cr, Ni, and Zr) in MG-Si are already below an important maximum limit for the SoG-Si feedstock calculated by Bathey and Cretella [16]. To decrease the concentrations of Fe, Ti, and V below this limit, however, directional solidification must be carried out at the lowest mold velocities (5 and 10 $\mu m\,s^{-1}$). This is not true for the Al concentration, which is still above this limit even after the directional solidification step. In the RMG-Si, the concentration of all elements except Al is already below this requirement before directional solidification. The Al content can be sufficiently reduced at the ingot bottom after directional solidification at the mold velocity of 10 $\mu m\,s^{-1}$. Some impurities, such as Al in the ingots obtained from RMG-Si, and Cu, Mn, Ni, Fe, and Ti in the ingots obtained from both types of feedstock (MG-Si and RMG-Si) at the lowest mold velocities are also below important concentration limits defined directly for SoG-Si, rather than for its feedstock.

Acknowledgements

The authors thank the financial support from Fundação de Amparo à Pesquisa do Estado de São Paulo (FAPESP) for grants 03/14118-1 and 03/08576-7, Conselho Nacional de Desenvolvimento Científico e Tecnológico (CNPq) for grant 475451/04-0, and Laboratory of Metallurgy and Ceramics Materials, Institute for Technological Research (IPT) for the scholarship to one of the authors (T.S.O.)

References

[1] E. Øvrelid, M. Juel, M. Bellmann, B. AgyeiTuffour, Silicon for the Chemical and Solar Industry IX, Oslo, Norway, 2008, pp. 91–101.
[2] A.F.B. Braga, S.P. Moreira, P.R. Zampieri, J.M.G. Bacchin, P.R. Mei, Sol. Energy Mater. Sol. Cells 92 (2008) 418–424.
[3] D. Lynch, JOM 61 (2009) 41–48.
[4] H. Kawamoto, K. Okuwada, Sci. Technol. Trends: Q. Rev. (2007) 38–50.
[5] A. Muller, M. Ghosh, R. Sonnenschein, P. Woditsch, Mater. Sci. Eng. B 134 (2006) 257–262.
[6] P. Woditsch, W. Koch, Sol. Energy Mater. Sol. Cells 72 (2002) 11–26.
[7] S. Pizzini, M. Acciarri, S. Binetti, Phys. Status Solidi A 202 (2005) 2928–2942.
[8] A.A. Istratov, T. Buonassisi, M.D. Pickett, M. Heuer, E.R. Weber, Mater. Sci. Eng. B 134 (2006) 282–286.
[9] S. Pizzini, Appl. Phys. A: Mater. Sci. Process. 96 (2009) 171–188.
[10] S. Pizzini, Sol. Energy Mater. Sol. Cells 94 (2010) 1528–1533.
[11] D. Sarti, R. Einhaus, Sol. Energy Mater. Sol. Cells 72 (2002) 27–40.
[12] J. Hofstetter, J.F. Lelievre, C. del Canizo, A. Luque, Mater. Sci. Eng. B 159–60 (2009) 299–304.
[13] E. Øvrelid, B. Geerligs, A. Waernes, O. Raaness, I. Solheim, R. Jensen, K. Tang, S. Santeen, B. Wiersma, in: H.A. Øye, H. Brekken, T. Foosnaes, L. Nygaard (Eds.), Silicon for the Chemical Industry VIII, Trondheim, Norway, 2006, pp. 1–12.
[14] N. Yuge, M. Abe, K. Hanazawa, H. Baba, N. Nakamura, Y. Kato, Y. Sakaguchi, S. Hiwasa, F. Aratani, Prog. Photovoltaics 9 (2001) 203–209.
[15] S. Pizzini, Sol. Energy Mater. 6 (1982) 253–297.
[16] B.R. Bathey, M.C. Cretella, J. Mater. Sci. 17 (1982) 3077–3096.
[17] L.P. Hunt, J. Electrochem. Soc. 131 (1984) 1891–1896.
[18] R.H. Hopkins, R.G. Seidensticker, P. Raichoudhury, P.D. Blais, J.R. Mccormick, J. Cryst. Growth 42 (1977) 493–498.
[19] A. Luque, S. Hegedus, Handbook of Photovoltaic Science and Engineering, Wiley, Hoboken, NJ, 2003.

[20] T.L. Chu, G.A. Vanderleeden, H.I. Yoo, J. Electrochem. Soc. 125 (1978) 661–665.
[21] B.G. Gribov, K.V. Zinov'ev, Inorg. Mater. 39 (2003) 653–662.
[22] K. Morita, T. Miki, Intermetallics 11 (2003) 1111–1117.
[23] F.A. Trumbore, Bell Syst. Tech. J. 39 (1960) 205–233.
[24] S. Kobayashi, in: R. Hull (Ed.), Properties of Crystalline Silicon, INSPEC – The Institution of Electrical Engineers, London, 1999, pp. 16–22.
[25] B.C. Sim, K.H. Kim, H.W. Lee, J. Cryst. Growth 290 (2006) 665–669.
[26] T. Narushima, A. Yamashita, C. Ouchi, Y. Iguchi, Mater. Trans. 43 (2002) 2120–2124.
[27] S. Martinuzzi, I. Perichaud, C. Trassy, J. Degoulange, Prog. Photovoltaics 17 (2009) 297–305.
[28] J. Degoulange, I. Perichaud, C. Trassy, S. Martinuzzi, Sol. Energy Mater. Sol. Cells 92 (2008) 1269–1273.
[29] T.L. Chu, S.S. Chu, R.W. Kelm, G.W. Wakefield, J. Electrochem. Soc. 125 (1978) 595–597.
[30] E. Kuroda, T. Saitoh, J. Cryst. Growth 47 (1979) 251–260.
[31] C.P. Khattak, M. Basaran, F. Schmid, R.V. D'Aiello, P.H. Robinson, A.H. Firester, Metallurgical Silicon Substrates Produced by Hem for Epitaxial Thin Film Solar Cells, 15th IEEE Photovoltaic Specialists Conference, Orlando, 1981, p. 1432.
[32] C.P. Khattak, D.B. Joyce, F. Schmid, Sol. Energy Mater. Sol. Cells 74 (2002) 77–89.
[33] N. Yuge, H. Baba, Y. Sakaguchi, K. Nishikawa, H. Terashima, F. Aratani, Sol. Energy Mater. Sol. Cells 34 (1994) 243–250.
[34] L.A. Currie, Pure Appl. Chem. 67 (1995) 1699–1723.
[35] W. Kurz, D.J. Fisher, Fundamentals of Solidification, 3rd ed., Trans Tech Publications, Aedermannsdorf, 1989.
[36] G.C. Vogelaar, in: H.A. Øye, H.M. Rong, B. Ceccaroli, L. Nygaard, J.K. Tuset (Eds.), Silicon for the Chemical Industry III, Sandefjord, Norway, 1996, pp. 95–112.
[37] M.C. Flemings, Solidification Processing, McGraw-Hill, New York, 1974.
[38] F.V. Dean, A. Hellawell, J.R. Kerr, J. Inst. Metals 90 (1962) 234–237.
[39] J.A. Burton, R.C. Prim, W.P. Slichter, J. Chem. Phys. 21 (1953) 1987–1991.
[40] A.S. Yue, J.B. Clark, Trans. AIME 218 (1960) 55–58.